JOURNAL OF THE MECHANICAL BEHAVIOR OF BIOMEDICAL MATERIALS 29 (2014) 138–150

Available online at www.sciencedirect.com

ScienceDirect

www.elsevier.com/locate/jmbbm

Research Paper

Solid–extracellular fluid interaction and damage in the mechanical response of rat brain tissue under confined compression

Henry W. Haslach Jr[a,*], *Lauren N. Leahy*[a], *Peter Riley*[a], *Rao Gullapalli*[c], *Su Xu*[c], *Adam H. Hsieh*[b]

[a]*Department of Mechanical Engineering, University of Maryland, College Park, MD 20742, USA*
[b]*Fischell Department of Biomechanical Engineering, University of Maryland, College Park, MD 20742, USA*
[c]*Department of Diagnostic Radiology & Nuclear Medicine, University of Maryland School of Medicine, Baltimore, MD 21201, USA*

ARTICLE INFO

Article history:
Received 2 May 2013
Received in revised form
22 August 2013
Accepted 27 August 2013
Available online 17 September 2013

Keywords:
Brain tissue damage
Confined compression
Solid–fluid interaction
Extracellular fluid
Models of injury
Permeability
Rat brain

ABSTRACT

The mechanical processes that underlie mild traumatic brain injury from physical insults are not well understood. One aspect in particular that has not been examined is the tissue fluid, which is known to be critical in the mechanical function of other organs. To investigate the contributions of solid–fluid interactions to brain tissue mechanics, we performed confined compression tests, that force the extracellular fluid (ECF) to flow in the direction of the deformation, on 6.35 mm diameter, 3 mm long cylindrical samples excised from various regions of rat brains. Two types of tests in deformation control, (1) quasi-static, slow and moderate constant strain rate tests at 0.64×10^{-5}/s, 0.001/s and 1/s to large strains and (2) several applications of slow linear deformation to 5% strain each followed by stress relaxation are employed to explore the solid–fluid interaction. At slow and moderate compressive strain rates, we observed stress peaks in the applied strain range at about 11%, whose magnitudes exhibited statistically significant dependence on strain rate. These data suggest that the ECF carries load until the tissue is sufficiently damaged to permit pathological fluid flow. Under the slow ramp rate in the ramp-relaxation cycles protocol, commonly used to estimate permeability, the stress relaxes to zero after the first cycle, rather than to a non-zero equilibrium stress corresponding to the applied strain, which further implicates mechanical damage. Magnetic resonance imaging (MRI) of changes in tissue microstructure during confined compression, before and after compression, provides further evidence of tissue damage. The solid–fluid interactions, reflected in the morphology of the stress–stretch curves and supported by the MRI data, suggest that increases in hydrostatic pressure in the ECF may contribute to mechanical damage of brain tissue.

*Corresponding author. Tel.: +1 301 405 8865; fax: +1 301 314 9477.
E-mail address: haslach@umd.edu (H.W. Haslach Jr).

1751-6161/$ - see front matter © 2013 Elsevier Ltd. All rights reserved.
http://dx.doi.org/10.1016/j.jmbbm.2013.08.027

1. Introduction

Subtle small-scale mechanical damage mechanisms in brain tissue that can modify brain function may be involved in the initial cause of mild traumatic brain injury (mTBI). Exposure to an external blast or to an impact may induce in the brain tissue a deformation wave whose longitudinal component compresses the tissue, and compression is known to induce cell damage in brain cell cultures (Cullen et al., 2011). Here we focus on the mechanical effect of compression on the integrity of the brain tissue rather than on shearing as might result from the shear component of the wave. Often overlooked in mechanical testing is the fact that brain tissue is biphasic, composed of water and solid phases, and its mechanical response is strongly influenced by the high fluid content of the brain tissue itself, whether extracellular or intracellular. Brain tissue may have a different mechanical response than load-bearing soft tissue with high fluid content because of structural differences. Brain tissue carries little load in vivo, in contrast to other soft tissues, such as cartilage or arteries, which are structured to return to the original configuration without damage after normal physiological deformation.

The configuration of brain tissue is maintained by interaction between the cellular solid matter and the brain extracellular fluid (ECF). The pattern of links between neurons, astrocytes and each other forms a mechanically weak network structure that maintains, along with the capillaries, the structural integrity of the brain by a combination of tension in axons, dendrites, and glial processes that is balanced by hydrostatic pressure in the ECF (Van Essen, 1997). Under mechanical deformation, disruption of the equilibrium balance of tension in the axons, dendrites and glial processes with the ECF hydrostatic pressure may lead to mechanical damage. One possible related mechanism is excessive axonal strain because stretch tests on isolated neurons show that the critical axonal tensile strain for axonal damage is about 20% (Bain and Meaney, 2000).

Brain injuries have been associated with the internal stress and strain that the brain undergoes during an external insult. However, no technique is available to determine the stress–strain relation inside the brain in vivo during the insult. In order to improve our understanding of these internal phenomena, the confined compression test can be used to investigate uniaxial solid–fluid interaction in the biphasic tissue. Confined compression testing offers advantages over experimental techniques that others have used to investigate the mechanical properties of brain tissue because a confined compression test, which may be idealized as uniaxial, applies a uniaxial deformation and ensures nearly parallel uniaxial flow of the ECF under the load. Interpretations of fluid flow cannot be made analytically from unconfined compression tests, which have traditionally been used to obtain uniaxial data for brain tissue (e.g. Prevost et al., 2011; Miller and Chinzei, 2002; Prange and Margulies, 2002), because in such tests fluid can move in bulk flow transversely to the direction of compression. Also, the unconfined compression test and the confined compression test have different boundary conditions. The internal fluid flow in confined compression is commonly assumed to be uniaxial to estimate the permeability of load-bearing soft tissue like cartilage (e.g. Ateshian et al., 1997), but the test rarely has been applied to brain tissue.

In this study, we investigate the mechanical response to compression of brain tissues from rats, which are routinely used in brain tissue research. Here the confined compression test is employed to explore the influence of fluid content on the uniaxial compressive deformation of rat brain tissue and to attempt a computation of the permeability coefficient. Our hypothesis is that some aspects of the non-equilibrium mechanical response of brain tissue to compression are due to solid–fluid interactions that depend on changes in the ECF hydrostatic pressure and that may induce tissue damage, in contrast to load-bearing soft tissue such as cartilage.

Standard techniques of measuring damage do not apply to our tests that seek the transient initial response to compression. Subsequent cyclic loading is not useful because brain tissue differs from load-bearing soft tissue, such as cartilage or arteries, in that a single load application of moderate strain can change its mechanical properties, as we show. Similarly, preconditioning specimens to reach a steady state (e.g. Cheng and Bilston, 2007) eliminates the transient response. Another common practice is to verify soft tissue damage using histology, but reported applications to brain tissue suggest that histology might not detect the subtle rearrangement of substructures that may be involved in our tests (e.g. Shulyakov et al., 2009; Prange and Margulies, 2002), as opposed to severe loads for which silver staining captures axoplasm flow from the severed ends of axons (e.g. Strich, 1961). Our main alternative technique examines the morphology of stress–stretch curves for the compressive response that may include indicators of damage, such as spikes on the curve due to reaction force drops, peaks in the stress, relaxation of the tissue to zero stress, and softening. The assumption is that many types of biodamage alter the stress carrying capability of the brain tissue. Changes in permeability may also indicate damage. Since dynamic imaging of the substructures of the brain during injury is not currently possible, we statically apply diffusion MRI after deformation to seek further indicators of damage. These results suggest that the confined compression test might serve as a useful in vitro model for studying fluid–solid related damage. The tests presented establish a baseline that may be later compared to the mechanical response under high strain rate deformation of brain tissue.

2. Methods and materials

2.1. *Specimen preparation*

Whole rat brains were harvested from freshly euthanized Sprague Dawley rats (6–9 months), whose brains are approximately 2 cm long and 1.2 cm wide. To produce 6 specimens from each rat brain for the confined compression tests, the specimens are carefully dissected using a scalpel, guided by a specially built fixture, to slice four 3 mm thick sagittal planar slabs from the cerebrum, two from each hemisphere, and two 3 mm thick frontal planar slabs from the cerebellum. Tissue slices were placed in Phosphate Buffered Saline (PBS) to

maintain hydration. One cylindrical specimen for the confined compression test is cut from each planar slab by a cylindrical hollow punch of inner diameter 6.35 mm (1/4 in.). The specimens from all three regions contain white matter; it is not possible to determine the precise proportion of white and grey matter in a given specimen without destroying the sample. Both the inner and outer sagittal specimens are taken from regions of the slice near the hippocampus and the corpus callosum where white matter dominates. The relatively large size of the heterogeneous cerebral specimens punched from the center of sagittal cerebrum slabs (Fig. 1a), as well as the frontal cerebellum specimens, allows the results more general application to the response of the full brain because each specimen includes interfaces between white and grey regions. Researchers seeking information about a particular brain region, usually white matter, have commonly excised a small number of uniform specimens from that region in a brain of a larger mammal such as a pig, sheep or cow.

2.2. *Water content measurement*

After measuring the wet weight, the dry weight of a complete rat brain is determined 1 day after harvest and storage in PBS at 4 °C by lyophilizing the brain tissue (Labconco, Kansas City, MO). The weights were measured on a balance (XS205, Mettler Toledo, Columbus, OH), which reads to 0.0001 g. Water content fraction by weight was calculated by $m = (\text{wet weight} - \text{dry weight})/\text{wet weight}$.

2.3. *Confined compression*

The specially designed and built fixture (Fig. 1b) encloses the specimen in an impermeable hollow, precision-machined, stainless steel cylinder of nominal inner diameter 6.35 mm (0.2503, tolerance 0.0003 in.) that prevents lateral deformation and accepts specimens of 6.35 mm in diameter and any length of up to 1 cm. So that the load and fluid flow are both uniaxial, a fixed porous stainless steel disk base allows fluid transport from the specimen as does the load applying porous hollow-cup stainless steel plunger (Mott, PN 1201900-01-400; 0.250 in. OD × 0.125 in. ID × 0.750 in. L) of mass 2.02 g attached to a shaft having mass 2 g and diameter 0.2485 in. The sintered porous 316L stainless steel plunger and base disk are, respectively, 40 and 20 media grade. Media grade as defined by the manufacturer, Mott Corp., is approximately the outer diameter in micrometers of particles in a liquid stream that the filter can stop 90% of the time as determined by a bubble point test. The permeability values provided by Mott for water flow through these media grades are on the order of 10^{-1}.

When the fixture is assembled for a test, the confinement cylinder rests on, but is not attached to, the porous base disk to allow insertion of the specimen from the bottom of the cylinder. To insert a specimen, the confinement cylinder is slipped out of the base cylinder. The hollow punch cylinder, which has sharpened edges, is forced into a slice of the brain tissue of the desired thickness so that a cylinder of matter remains inside the hollow punch. The stainless steel punch inner diameter tolerance is the same as that of the confinement cylinder. The plunger shaft is inserted into the confinement cylinder and is pushed through enough that the plunger end extends out of the cylinder. The specimen is transferred from inside the punch to the tip of the plunger to which it sticks so that the specimen may be easily withdrawn from inside the punch cylinder without otherwise being touched. The plunger shaft is withdrawn enough that the face of the specimen is at the bottom of the confinement cylinder. The containment cylinder with the plunger shaft inside is inserted into a base support so that its end and the face of the specimen

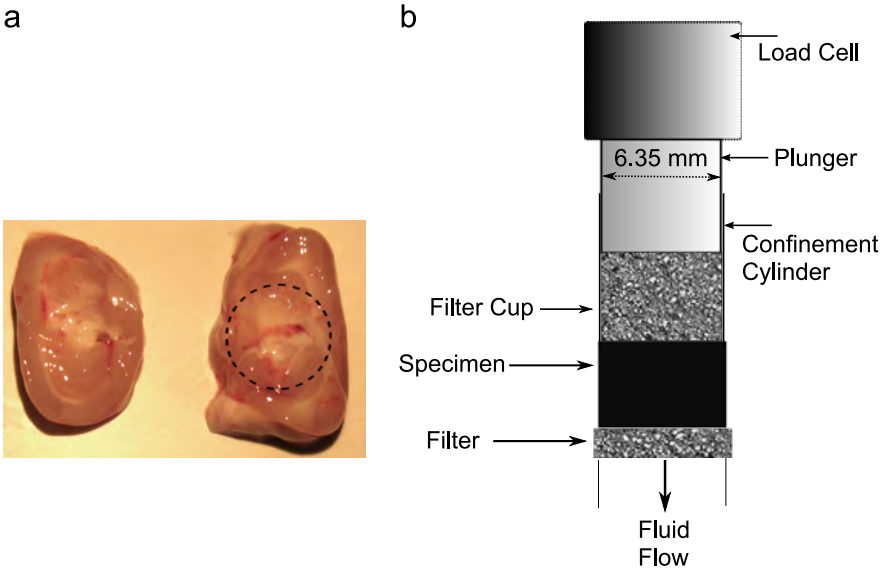

Fig. 1 – (a) The left image is the outer slab and the right is the inner slab of one hemisphere of a rat cerebrum. One heterogeneous specimen is punched from the center of each slab. The dotted circle indicates the boundary of the cylindrical specimen punched from the inner slab on the right. The visible surface in the left slab is placed adjacent to the plunger, and the visible surface of the right slab is at the base. (b) Schematic of the confined compression apparatus, with 6.35 mm (0.25 inch) inner diameter of cylinder, where h is the specimen length and Z is the coordinate in the reference system.

touch the base porous disk. The end of the cylindrical specimen placed next to the plunger is always the medial surface of the sagittal slice, because this surface contains a larger proportion of white matter substructures. Two ring weights of 12.5 g each, which do not touch the plunger, are placed on top rim of the confinement cylinder to prevent forced radial flow of tissue material between the porous base disk and the underneath of the bottom of the confinement cylinder when the tissue is excessively squeezed. After each test, the confinement cylinder is removed and inspected to verify that no material has leaked. The insertion of the specimen process takes less than 2 min.

The load is applied in deformation control by a Bose-Electroforce Testbench 200 N machine that can provide a maximum 100G acceleration, 3.2 m/s deformation rate and 400 Hz sinusoidal frequency; the software was Wintest 2.0 and 4.1. A Bose 250 g load cell at low strain rates or a Bose 22 N load cell at higher strain rates measures the reaction force at the plunger contact with the specimen. The masses of the either load cell and plunger total less than 79 g; the Bose specification LM-1 Testbench manual indicates that an inertial load up to 1600 g attached to the motor does not affect the response at speeds up to 20 Hz. Before the test loading is begun, the end of the plunger shaft is brought into contact with the Bose mover with a tare load of 1 g. All specimens are tested in the laboratory environment of 21 °C and 30% relative humidity, within 4 h of rat euthanasia.

Specimens were excised from 17 fresh rat brains and one frozen brain, one brain per test session, but not all specimens were used for these confined compression tests. Specimens are rejected if voids are visible on the ends of the cylindrical specimen, if tissue leaks from underneath the confining cylinder in spite of the precautions or if the control software malfunctions. One of the six quasi-static, 5 of 14 slow rate, 4 of 15 fast rate, and 3 of 12 repeated load-relaxation tests were rejected for these reasons.

Two protocols are employed for the confined compression tests. In the first protocol, the deformation is increased linearly until a 25% global strain is exceeded at strain rates that are quasi-static, slow (0.001/s), and moderate (1/s). The strain rate of 0.64×10^{-5}/s for quasi-static tests to obtain the equilibrium stress–stretch relation was chosen to match the porcine brain test rate in unconfined compression of Miller and Chinzei (1997, 2002).

In the second protocol, in an attempt to compute the tissue permeability by the same technique used for cartilage (e.g. Ateshian et al., 1997), cycles of a ramp deformation followed by relaxation were applied. The specimen is subjected to a linearly increasing deformation at a constant rate until the plunger has moved through 5% of the original specimen length. The plunger is held fixed so that the applied deformation is constant, and the reaction force at the plunger is allowed to relax for a fixed period of time or until the relaxation load changes less than 0.5 g. Then the specimen is subjected to an additional 5% global strain superposed on the original 5% strain so that the total strain from the beginning of the test is 10%, and the deformation is held constant while the specimen stress relaxes. This cycle is repeated for global total strains of 15, 20, and 25% for which the reference configuration is always the original specimen.

The stress is the measured force divided by the 31.67 mm^2 cross-sectional area of the specimen, and the stretch, λ, is equal to $1+\varepsilon$, where $\varepsilon \le 0$ is the global compressive engineering strain computed as the deformation at the plunger divided by the original length of the specimen. Therefore the undeformed state is $\lambda = 1$ and the compressive stretches are $0 < \lambda < 1$. The stress–stretch curves obtained here for a given set of conditions are not averaged because averaging would obscure the transient response and would remove the worst-case possibility, which would be required in any application to brain injury. Further, stress variation from test to test arises from the small size of the excised specimens forced by the small size of the rat brain and the desire to obtain data from each brain region.

2.4. *Magnetic resonance imaging*

All MRI experiments are performed on a Bruker BioSpec 70/30USR Avance III 7 T horizontal bore MR scanner (Bruker Biospin MRI GmbH, Germany) equipped with a BGA12S gradient system and interfaced to a Bruker Paravision 5.1 console. A Bruker 72 mm linear-volume coil is used as transmitter and receiver.

A 6 mm long, 6.35 mm diameter cylinder of brain tissue is placed in a polycarbonate replica of the confined compression fixture in the imaging coil and centered in the magnet. MRI experiments are performed before and after compression to 10% strain.

A three-slice (axial, mid-sagittal, and coronal) scout using fast low angle shot (FLASH) sequence is obtained to localize the sample. Proton density-weighted images for anatomic reference are obtained using a 2D rapid acquisition with relaxation enhancement (RARE) sequence covering the entire sample. The acquisition parameters are TR/TE_{eff} of 5500/19 ms (TR is the inter-pulse repetition time and TE is the echo time), RARE factor of 4, field of view (FOV) of 12×12 mm^2, slice thickness of 0.5 mm, in-plane resolution of 150×150 μm^2, with 22 averages. The acquisition time is just under 33 min. T_2 maps are generated using a sixteen-echo multi-echo spin echo pulse sequence with the TE of the first echo at 11 ms (TR=2696 ms), and the inter-echo spacing is also 11 ms. These images are obtained with 1 mm slice thickness covering the entire tissue in about 15 min. Following the acquisition, T_2 maps are calculated by Bruker Paravision 5.1.

Diffusion tensor images are acquired with a spin-echo sequence. Diffusion sensitive gradients are applied in 6 directions at $B=2000$ s/mm^2. The acquisition parameters are TR/TE of 2500/23 ms, in-plane resolution of 160×160 μm^2, number of average of 2, slice thickness of 1 mm, and cover the same area as the T_2 mapping experiment in about 44 min. Following the acquisition, the mean diffusivity (MD) and fractional anisotropy (FA), which indicates the anisotropy of the diffusion process, are calculated by Bruker Paravision 5.1.

3. Results

The water content of rat brain tissue is large enough that its influence on the mechanical response cannot be ignored. The wet weight of one complete rat brain just prior to beginning lyophilizing was 2.499 g and the final dry weight was 0.462 g. Therefore the water content fraction by weight is $m=0.815$,

but that may have been increased slightly by the initial storage in PBS. The proportion of the water from the cerebrospinal fluid and from the extracellular and intracellular fluid is unknown.

3.1. *Stress–stretch relations in compression*

A quasi-static test at the very small strain rate 0.64×10^{-5}/s assumes that the material moves through a sequence of equilibrium states. A quasi-static curve (Fig. 2a) describing the response of a specimen excised from the inner sagittal plane of the cerebrum exhibits multiple spikes due to drops in the stress magnitude beginning at small global strains of less than 5%. These drops in stress are common in soft tissue biomechanical testing and are typically indicative of subfailure tissue damage (e.g. Burgin and Aspden, 2008; Noyes et al., 1984). In contrast, a similar 0.64×10^{-5}/s quasi-static test of a 4% agarose gel specimen in the confined compression apparatus produces a smooth curve (Fig. 2b).

The only path for moisture to evaporate into the ambient laboratory atmosphere is the less than 0.00304 cm^2 area allowed by the tolerance separation between the plunger and the confinement cylinder. The change in weight due to evaporation of a 0.109 g specimen left unloaded in the apparatus for 21 h was 0.014 g as read on a Mettler Toledo PB403-S balance. Proportionally, the estimated change in weight in the 4.82 h required to reach 11% strain is 0.00321 g or a weight loss of about 2.9%. Therefore the influence of evaporation on the quasi-static stress–stretch response is likely to be small.

The stress at −0.11 strain ($\lambda = 0.89$) is given in Table 1 from five quasi-static tests for comparison to the peak stress data given below in Table 2. Table 1 includes the five successful quasi-static tests of the six conducted; each of the specimens was from different rat brains so that the variation in stress at 11% strain may be due to individual animal differences. In all Tables, the region denoted by inner (outer) indicates a cylinder punched from an inner (outer) sagittal slice of the cerebrum. The (R) or (F) indicates a specimen punched from the rear (front) frontal plane of the cerebellum.

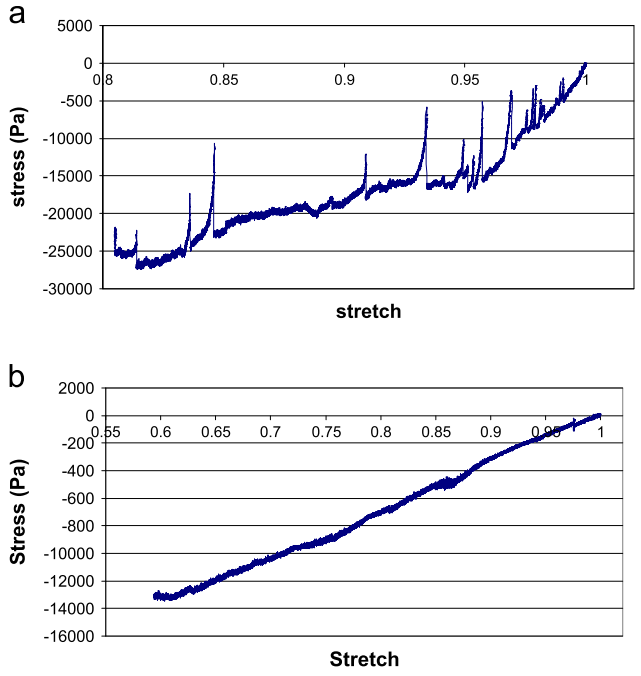

Fig. 2 – (a) Quasi-static stress–stretch curve at a strain rate of 0.64×10^{-5}/s from Rat1e (Table 1). (b) Quasi-static stress–stretch curve in confined compression at a strain rate of 0.64×10^{-5}/s for 4% agarose gel.

Table 1 – Compressive quasi-static stress at −0.11 strain.

Specimen	Region	Stress (kPa)
Rat1e	Inner	−19.9
Rat2e	Inner	−40.0
Rat3e	Outer	−24.1
Rat4f	Outer	−18.6
Rat5f	Cerebellum (R)	−27.3
Average (SD)		−26.0 (−8.60)

Constant deformation rate compression tests, in addition to the quasi-static tests, were performed at the slow strain rate of 0.001/s and a moderate rate of 1/s, a six decade range from quasi-static to moderate rates. The most significant feature of the slow and moderate rate curves (Figs. 3 and 4) is that the stress increases until it reaches a peak and then drops to a plateau or gradually decreases, a behavior that does not appear on any quasi-static stress–stretch curve. Table 2 reports the peak stress and corresponding stretch for the 9 successful out of 14 slow rate tests and the 11 successful out of 15 moderate rate tests. At both strain rates, the peak stress often occurs at nearly the same strain, while the peak stress is greater in the moderate rate tests than in the slow rate tests (Table 2). The average peak stress for 0.001/s is 86.6 kPa (SD=63.2) at an average strain of −12.9% ($\lambda = 0.871$, SD=9.65%) and the average peak stress for 1/s is 251.6 kPa (SD=134.4) at an average strain of −10.88% ($\lambda = 0.8912$, SD=5.13%). In each case the coefficient of variation, the standard deviation divided by the mean, is less than one, indicating moderate variation of the results. Single factor ANOVA with critical p value of $\alpha = 0.05$ shows that the difference in peak stress magnitude between the two rates is statistically significant ($F=9.09$, $p=0.008$), while the difference in the strain at the peak stress is not ($F=0.33$, $p=0.573$). The response to deformation is rate-dependent.

The average stress at −0.11 global strain for the quasi-static tests reported in Table 1 is less than the average peak stress for the 0.001/s rate. No statistical difference is found between the response of the inner and outer specimens most likely because of their similar heterogeneity.

The existence of the peak stress on the stress–stretch curves for the ramp load suggests a method to estimate the permeability, k, of the tissue at the peak, which is a measure of the resistance to ECF flow. The permeability may depend on both the strain and the strain rate. Assume that, over the full specimen length, the fluid pressure drop magnitude across the solid component is approximately the peak stress magnitude, S, just before the solid is damaged enough that the permeability can rapidly increase. Assume that the velocity of the ECF, v, is approximately the velocity of the plunger motion. Then the permeability is approximately $k = vh/S$ from the steady Darcy relation, where h is the specimen length. The permeabilities estimated in this manner at the

Table 2 – Rate dependence of peak stress and strain in confined compression.

Specimen	Strain Rate (/s)	Region	Peak Stress (kPa)	Strain at Peak (%)
Rat6a	0.0004	Outer	−23	−5.5
Rat7a	0.00025	Cerebellum	−19	−2.6
Rat8a	0.001	Outer	−23	−1.7
Rat12b	0.001	Outer	−77	−9
Rat10d	0.001	Outer	−171	−20.9
Rat12c	0.001	Inner	−95	−11.7
Rat13c	0.001	Inner	−169	−16.1
Rat12a	0.001	Cerebellum (R)	−57	−2.5
Rat13e	0.001	Cerebellum (R)	−15.9	−28.2
Rat9c	1.0	Outer	−245	−14
Rat10a	1.0	Outer	−225	−9
Rat9d	1.0	Outer	−242	−10
Rat9e	1.0	Inner	−122	−12
Rat10b	1.0	Inner	−450	−9
Rat10c	1.0	Inner	−255	−7
Rat14d	1.0	Inner	−231	−6.3
Rat11c	1.0	Cerebellum (F)	−140	−6
Rat14e	1.0	Cerebellum (F)	−547	−24.4
Rat10f	1.0	Cerebellum (R)	−101	−12
Rat11d	1.0	Cerebellum (R)	−240	−10

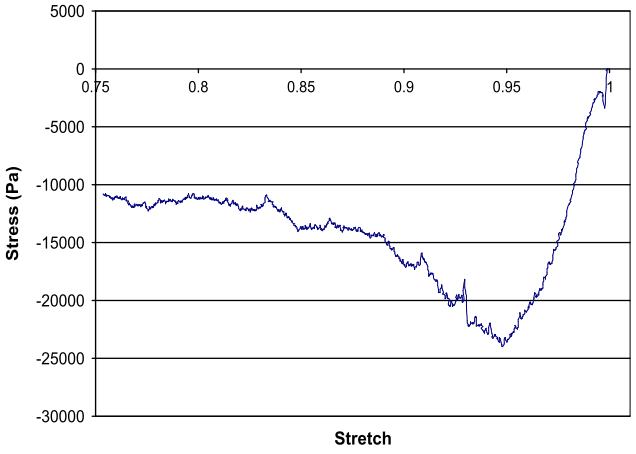

Fig. 3 – Typical stress–stretch curve at 0.001 mm/s (0.0004/s) from Rat6a (Table 2) that shows a stress peak and plateau in the response.

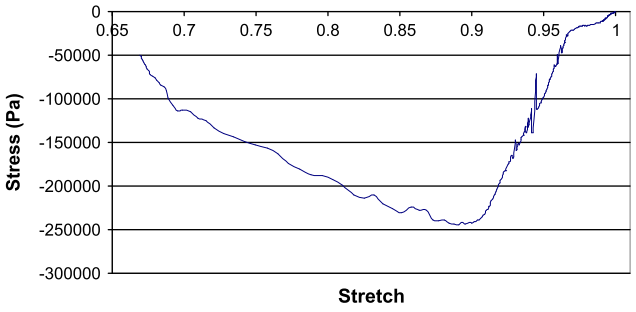

Fig. 4 – Typical stress response at the moderate strain rate 1/s from Rat9d (Table 2) showing the peak stress and subsequent decrease due to damage.

quasi-static 11% strain, and at the slow and moderate strain rate peaks of a 3 mm long specimen are respectively, 2.22×10^{-15}, 1.038×10^{-11}, and 3.56×10^{-9} m^4/Ns, all of which are

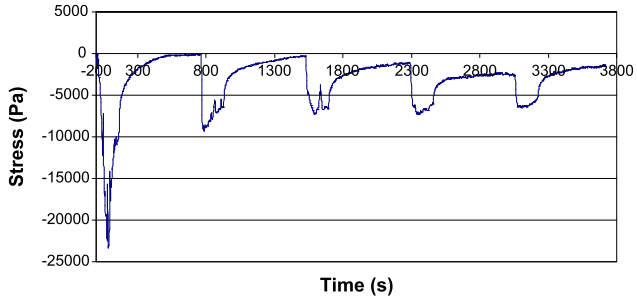

Fig. 5 – Typical load-relaxation curve (Rat15c); the ramp was obtained by deforming the specimen at 0.001 mm/s to produce a 0.00296/s strain rate. Relaxation to zero stress occurs on the first two deformation cycles.

in the range of the values given by others (Franceschini et al., 2006; Kaczmarek et al., 1997; Cheng and Bilston, 2007).

3.2. *The response to load-relaxation cycles*

The load-relaxation experiment as described in the methods section deforms the specimen by moving the plunger to 5% of the original specimen length at a constant rate, allows the specimen to stress relax and repeats several times this cycle of superposition of an additional 5% global strain on the previous strain followed by relaxation. The load-relaxation cyclic tests were planned to measure the strain-dependence of the permeability of brain tissue but also to provide additional indicators of mechanical damage that occurs during the ramp load. The indicators are the equilibrium stress achieved after relaxation, the time required to reach equilibrium, and the stress–stretch relation of the ramp loading before and after a relaxation. The curve in Fig. 5 is a typical stress versus time response showing drops in stress during the each ramp portion of the loading followed by an exponential type relaxation curve.

At the end of a ramp load, the specimen is not uniformly strained prior to relaxation. The biphasic theory, often applied to cartilage, predicts that during stress relaxation under a fixed plunger deformation the strain relaxes to a uniform value in the specimen equal to that at the plunger. This strain and the final relaxation stress are the equilibrium state of undamaged tissue. However, the response of brain tissue, an in vivo non-load bearing material, seems to differ from that of a naturally load bearing material like cartilage. We find that a specimen with stress drops during the ramp load portion can relax to values lower than the equilibrium stress corresponding to the global strain at the end of the plunger displacement as measured in the quasi-static tests, including zero, in contrast to the behavior of undamaged cartilage (Ateshian et al., 1997). Specimens cycled five times in 5% reference strain increments typically stress relax to zero on the first and second cycles (Table 3) rather than to the equilibrium stress corresponding to the constant global strain, and such relaxation to zero stress occurs in specimens excised from all regions of the brain. Specimens compressed at the slow rate relax to zero after the initial relaxation cycles but then relax to a non-zero stress on later relaxation cycles. When the next ramp deformation leads to a non-zero reaction stress at the plunger, it closely reproduces the pattern of an increasing load response that plateaus. The stresses at the peak loads at the end of the ramp loadings in the cycle may not increase in a sequence corresponding to the increase in global strain with respect to the original specimen length. In fact they often decrease, suggesting that the previous loading has lowered the maximum load-carrying capability of the rat brain tissue. The original equilibrium stress–strain relation for the solid cannot be obtained from the relaxation curves, as done for cartilage (e.g. Fig. 3 of Ateshian et al., 1997).

The relaxation response observed in the slow rate load-relaxation tests is summarized in Table 3, which reports the successful 9 of the 12 tests attempted, where the column called “cycles to 0” refers to the cycles on which the stress relaxed to zero.

We postulate that the time for relaxation to a nearly constant stress may be a measure of the amount of damage that occurred in the previous ramp load. The average relaxation time to zero stress after the first ramp of the slow rate tests from Table 3 is 439.3 s (SD 229.6 s).

The linear biphasic model assumes constant permeability as an approximation, but the linear biphasic model of tissue with a linear elastic solid component does not fit the data from the rat brain. The brain tissue relaxes to a much smaller stress than predicted by the linear biphasic model (Soltz and Ateshian, 1998), corrected in Soltz and Ateshian (2006), as shown in Fig. 6 using the trust-region-dogleg algorithm (Matlab lsqcurvefit) to determine the permeability value yielding the best fit.

3.2.1. *Stress–stretch relation before and after relaxation*

The load-relaxation tests also give information about the mechanical effect of repeated loading, i.e. repeated exposure to insults. The relaxed material after a ramp deformation may best be considered a new material since its substructure has changed, with different material properties, after loading and relaxing. In contrast, the properties of a load-bearing material are not likely to change after loading into the physiological range because the tissue is structured to repeatedly perform its function.

The curves of Fig. 7 for a specimen (Rat15c) excised from the inner sagittal plane of the cerebrum, and for which the ramp load is applied at a strain rate of 0.000296/s (0.001 mm/s), are found by calculating the stress versus strain relation for each ramp loading. For this analysis, the normal

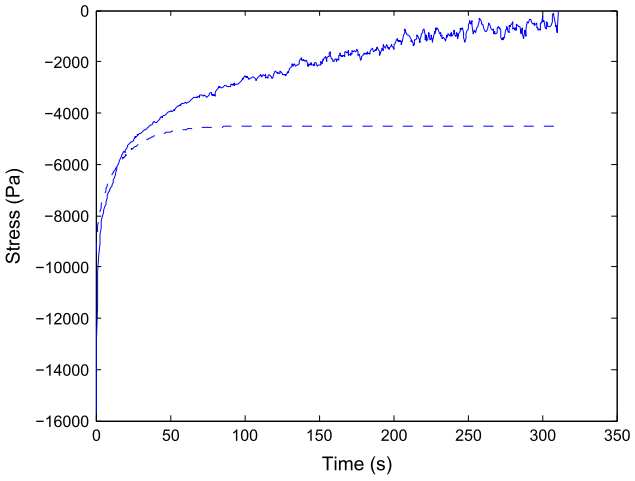

Fig. 6 – Brain tissue relaxes to a much lower stress than predicted by the linear biphasic partial differential equation. The solid curve is the brain relaxation data from a ramp deformed at 0.001/s (Rat17a), and the dotted line is the linear biphasic fit. The stress limit of the fit is −4500 Pa as expected since the elastic modulus of the hydrated tissue is assumed to be 90 kPa and the initial strain is −0.05. The product of the permeability and elastic modulus is 4.7392×10^{-8} from the initial guess of 1.4×10^{-8}.

Table 3 – Slow rate relaxation properties.

Specimen	Ramp strain rate (/s)	Region	Cycles to 0	Relaxation rime (s)
Rat15a	0.00033	Inner	1, 2, 3, 4, 5	300
Rat15c	0.000296	Inner	1, 2	390
Rat18d	0.001	Cerebellum	1	335
Rat19c	0.001	Cerebellum	1, 2, 3	724
Rat16f	0.001	Cerebellum	1, 2, 3, 4	132
Rat17a	0.001	Outer	1, 2	349
Rat19a	0.001	Outer	1, 2, 3	258
Rat18b	0.001	Inner	1, 2, 3	726
Rat19b	0.001	Inner	1	740

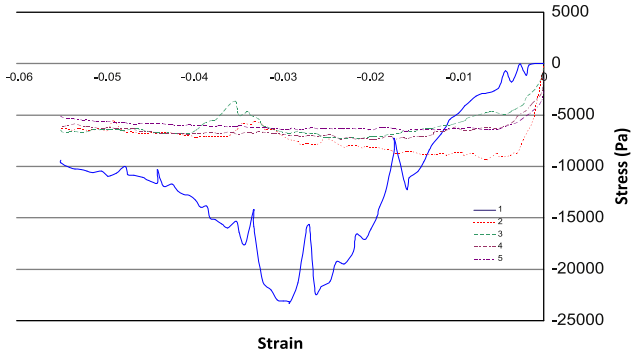

Fig. 7 – Stress–strain graphs of the successive increasing constant deformation ramps in Fig. 5 each treated as a new material. The curves approach a steady state on the fourth and fifth ramps.

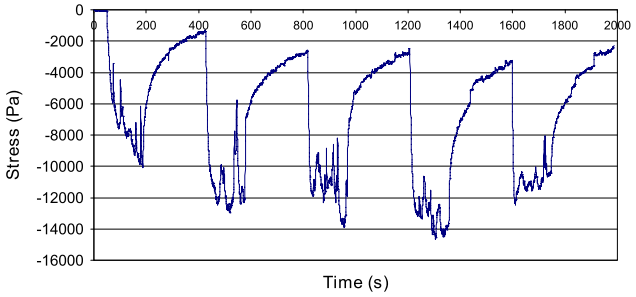

Fig. 8 – The load-relaxation cycle response of a specimen that had been frozen for storage and then thawed before testing. On the ramps, the specimen was deformed at 0.001 mm/s. Damage is shown by the spikes at the end of each ramp region. The specimen was not allowed to relax long enough to reach zero stress on the first few cycles.

strains in each ramp load are calculated by dividing the change in displacement of the plunger by the original length of the specimen, and to compare the behavior on each subsequent ramp, the stress–strain curves are plotted on the same coordinates (Fig. 7). Each ramp load is viewed as a new loading, and the displacement is re-set to zero at the beginning of each ramp so that the strain varies between 0 and −0.05. The stress is calculated by dividing the force detected with the load cell by the initial cross-sectional area of the specimen prior to any loading. The stress is not zeroed before each ramp load; however the first two cycles relax to zero stress (Fig. 5), while after the last three ramps the relaxation stress does not reach zero. As the strain increases, the stress on each ramp approaches an asymptote at about 5000 Pa. On the graph in Fig. 7, the limiting stress curve can be seen in the fourth and fifth cycles.

Freezing the tissue before testing, which is not recommended, provides more evidence that the tissue fluid plays a role in damage because freezing and then thawing for the test causes multiple spikes and multiple plateaus on the ramp portion of the load-relaxation response curve, as shown in a test at the slow strain rate of 0.00033/s (0.001 mm/s) (Fig. 8). This morphology could potentially be due to additional damage by volumetric expansion from ice formation.

3.3. *MRI evidence for tissue damage*

The largest changes in the tissue after compression, compared to the state prior to compression, are observed near the plunger and near the base, even though the viscoelastic tissue relaxed during the time required for imaging. Closer to the plunger, we observe a reduction in T_2 of about 9%. The reduction in T_2 is higher in the slices closest to the plunger side and on the base side suggesting that the higher forces at these locations expunge the free water and leave behind only bound water. Fig. 9 is an example of the images obtained, which yield the T_2-values of the tissue.

From the diffusion tensor imaging data (Table 4), variation in readings with position within the specimen prior to application of compression indicates that the brain tissue sample possesses heterogeneous properties. After the application of compression, each region of the sample exhibited changes that diagnostic radiology interprets as tissue damage. Closer to the plunger the fractional anisotropy (FA) is reduced by 5% and the mean diffusivity (MD) is reduced by 4% also indicating tighter spaces for water to diffuse. Similarly, the FA is also reduced at the base by 3% but without a change in mean diffusivity.

A decrease in fractional anisotropy of about 5% but with no changes in mean diffusivity in some areas indicates that the cell membranes are stretched and that water is being contained between the membranes. Near the plunger, the decrease in FA and a decrease in mean diffusivity suggest that, along with the membranes being stretched, there is also a large amount of cellular debris which restricts water mobility and hence reduces mean diffusivity. Overall, the effect is greater on the plunger side.

This explanation also correlates well with the T_2 data which shows that there is nearly a 10% reduction in T_2 values and suggests that there is a significant amount of bound water after being compressed. In other words the environment has become more rigid for any remaining free water.

Taken together, the results from T_2 measurements and from diffusion tensor measurements indicate that the tissue's microenvironment has changed significantly from its 'normative' uncompressed state. Compression, even at the relatively small strain of 10%, has modified the tissue in a manner that suggests damage.

4. Discussion

The morphology of our compressive stress–stretch curves suggests that a possible damage mechanism, other than shear, is excessive hydrostatic pressure in the ECF. The distinctive features of the stress–stretch response that we observed include sudden drops of the stress in response to a constantly increasing strain magnitude, peaks in the stress response, and stress relaxation to zero stress. These features are typical indicators of changes in the physical structure of the tissue, and may be attributed to solid–ECF interactions in the brain tissue. We postulate that the physical phenomena inducing these indicators are candidates for mechanical events that damage brain tissue.

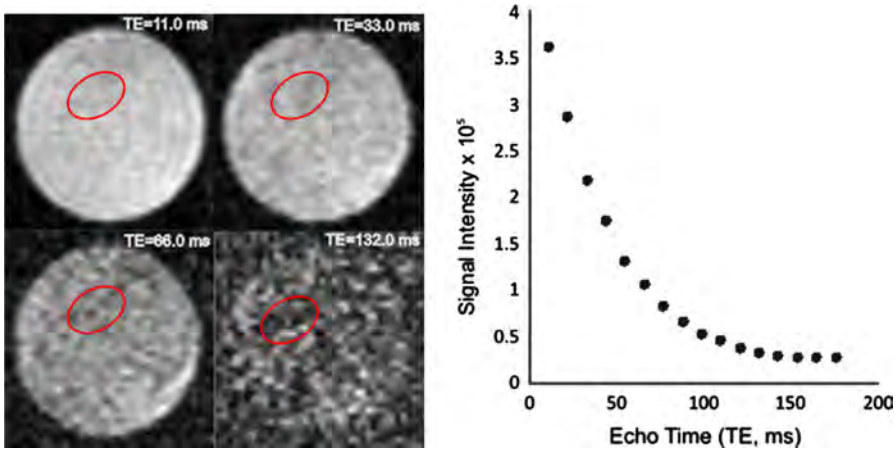

Fig. 9 – Left panel shows MR images of the brain tissue placed in the compression chamber from different echo times with the signal intensity decreasing exponentially with increasing echo time. The graph on the left shows the drop in signal intensity with echo time from the average of the pixels within the red oval in the figure on the left for each echo. Curve fitting is then performed to obtain the spin–spin relaxation time constant, T_2, of the tissue before and after compression. (For interpretation of the references to color in this figure caption, the reader is referred to the web version of this paper.)

Table 4 – Diffusion tensor imaging values from a specimen before and after confined compression.

	Base	Middle	Plunger
Pre-compression			
FA	0.955 ±0.195	0.939 ±0.207	0.917 ±0.212
MD ($\times 10^{-3}$ mm^2/s)	0.255 ±0.078	0.270 ±0.077	0.257 ±0.072
Post-compression			
FA	0.926 ±0.204	0.906 ±0.194	0.872 ±0.212
MD ($\times 10^{-3}$ mm^2/s)	0.255 ±0.069	0.276 ±0.065	0.247 ±0.059

4.1. *Evidence for solid–fluid interaction in the morphology of the ramp curves*

The mechanical response of a single-phase non-biological polymer typically depends on the behavior of its substructures, such as crystallization of the long-chain molecules induced by the load, but in a biphasic material, such as brain tissue, the fluid is also expected to affect the substructures.

The quasi-static curve of Fig. 2a shows occasional large sharp drops indicating that the specimen temporarily lost resistance to the constant deformation applied by the plunger. Because the specimens are heterogeneous, the stress drops may be a result of slip at the interface between grey and white matter, between axonal tracts or other subelements. The slip cannot occur spontaneously since the plunger is in deformation control, and therefore the drops in reaction force must be due to material slipping within the specimen, a rearrangement of substructures induced by redistribution of the ECF. The sudden drops in the curve are not due to sticking of the outside of the specimen to the wall of the containment cylinder because, if the specimen had stuck to the containment cylinder wall, the drops would have been preceded by a rapid increase in the force supported. These drops are characteristic of the heterogeneous brain tissue in confined compression as shown by the contrasting smooth curve obtained for a homogeneous agarose gel in Fig. 2b, tested within the same confined compression apparatus. The gel curve is not intended as a model for brain tissue, but to show that its curve has no spikes and that the apparatus allows a specimen to deform without sticking to the wall during compression. Further, in the fully enclosed chamber, a specimen can only compress, it cannot slip as a unit with respect to the wall. Dehydration due to evaporation during the quasi-static experiments up to 11% strain probably has at most a slight effect on the mechanical response, compared to the compression induced fluid loss, as shown by the small 2.9% weight loss in our evaporation test. The large sharp stress drops begin in the initial portion of the test before much dehydration is likely.

The strain rate dependence of the mechanical response of brain tissue to confined compression is most convincingly demonstrated by comparing the quasi-static curves to curves obtained at strain rates one thousand or one million times faster. One possible explanation for the ability of the brain tissue to support higher loads at a given stretch under higher rates is that the ECF supports more load because it is constrained by the tissue structure in a manner described in the following subsection.

While our quasi-static curves did not peak in the strain range tested, the curves at higher strain rates attain a peak stress and then decline with increasing global strain. Most load-bearing soft tissues, such as cartilage, do not peak in stress prior to strains up to 30%, but the interstitial fluid in cartilage does support a large portion of the load in the

increasing ramp segment of the confined compression tests of Soltz and Ateshian (1998). We postulate again that at the higher rate the peak is larger because the brain solid matter resists ECF transport and so the tissue carries more stress until the tissue is damaged enough that the permeability increases to allow ECF flow. Therefore, the observation that there is a strain rate-dependent increase in peak stress is further evidence of the role of ECF. If the peak stress were to indicate only weakening of adhesions in the solid material in the tissue, the peak values would likely be nearly the same at both rates. Interestingly, the slow and moderate rate test curves exhibit a major morphological change, the stress peak, at similar global compressive strain magnitudes of about 11%, a much smaller strain magnitude than the 21% tensile strain threshold reported for axonal injury under tensile tests of axons (Bain and Meaney, 2000). Because the stresses are statistically different at these rates, strain appears to be a better criterion for mechanical damage than stress.

Some regions of the stress–stretch curves at the various rates are concave up and others are concave down. A possible contributor to concavity is a change in permeability because the intervals where the curve is concave up (softening) indicate that the material provides less resistance to the constant deformation, possibly because the deformation has opened passageways for ECF motion. Typically, a biphasic material should harden if the permeability decreases with strain perhaps due to pore compaction that blocks passageways for ECF flow.

The permeability values computed for the slow and moderate rate tests at the average peak stress and at -0.11 strain in the quasi-static case increase with strain rate, suggesting that the higher strain rate ramp deformation has caused more damage as indicated by the larger permeability. Such a trend is consistent with the permeability measured for agarose gel at different strain rates (Liu et al., 2011).

Most brain tissue permeability values given in the literature are independent of strain. The Terzaghi consolidation theory based on small strains, a linearly elastic solid, and the Darcy relation has been used to estimate the permeability of human cortex tissue in vitro as 2.42×10^{-11} m/s (specific permeability $\sim2.4\times10^{-15}$ m^4/Ns) (Franceschini et al., 2006), a value smaller than other estimates. The permeability values of 1.6×10^{-11} m^4/Ns were chosen for white matter and 1.6×10^{-13} m^4/Ns for grey matter by Kaczmarek et al. (1997) in their finite element method model. Unconfined compression tests of white matter excised from the corpus callosum of calves have produced a constant permeability of 4.08×10^{-12} m^4/Ns (Cheng and Bilston, 2007), from specimens that were 20 mm in diameter and 4 mm thick, when computed by a poroelastic theory assuming a linear viscoelastic solid (e.g. Simon, 1992; Simon et al., 1998).

4.1.1. *A structural explanation for the morphology of the stress–stretch curves*

The brain tissue structure may explain the qualitative difference in the morphology of the stress–stretch curves as well as the different magnitudes of the stress as a function of deformation rate. Tissue structure may also explain the differing combined compression behavior of brain tissue from that observed in a load-bearing soft tissue like cartilage. Cartilage is composed of entangled collagen fibers and large proteoglycan macromolecules, as well as glycoproteins, chondrocytes, and some lipids (Mow et al., 1980). In contrast to the structure of brain tissue, the fibers form a network that preserves the integrity of the tissue so that the cartilage is undamaged during a confined compression test and does not exhibit the drops in stress on the ramp portion of the loading seen for brain tissue.

The cellular composition of the brain is nearly equal amounts of neurons and glia, such as astrocytes, as well as many small blood vessels, some collagen reinforced and blood-filled large blood vessels, and the brain extracellular fluid. In the absence of insults, the mechanically weak network structure of neurons and glia maintains the structural integrity of the brain by a balance of tension in axons, dendrites, and glial processes with the hydrostatic pressure in the ECF (Van Essen, 1997), rather than any extracellular framework. A thin perineuronal net (PNN) of extracellular matrix proteins does surround cellular substructures, but lacks major fibrous structural components (Bonneh-Barkay and Wiley, 2009). The PNN is believed to serve in a more regulatory role in limiting/directing synaptic contacts. As such, its composition and structure resembles the ground substance of soft tissues, which by itself is not amenable to supporting mechanical forces.

Two main hypotheses for cortical folding of the developing brain in some mammals are axonal tension (Van Essen, 1997) or intercortical differential growth (Xu et al., 2010). One aspect of the van Essen hypothesis not emphasized in this debate is that the morphology of the brain is maintained by a balance between axonal tension and hydrostatic pressure to substitute for the lack of a structural framework in brain tissue. Irrespective of which hypothesis is correct, other research supports the idea that axons are in tension in the mature brain. Dissection experiments have verified that axons in the undeformed mature mouse brain and the ferret brain are in significant tension (Xu et al., 2009, 2010). The mouse brain, as well as the rat brain, exhibits no cortical folding in the cerebrum while the ferret brain does. Quantitative tract tracing shows that the pattern of axonal trajectories is consistent with axonal tension and helps maintain the morphology of unloaded mature rhesus monkey prefrontal cortical tissue (Hilgetag and Barbas, 2006).

One plausible description of the mechanism underlying our stress–stretch curve morphology depends on the fact that the ECF, which is incompressible, supports load if the ECF is prevented from flowing by some tissue solid material. The ECF in the unloaded brain tissue is under an equilibrium hydrostatic pressure that balances the tension in the axon, dendrites, and glial processes to maintain the shape of the tissue, but applying deformation to the tissue disrupts this equilibrium balance. In the confined compression test to the magnitudes of deformation that we applied, fluid must exit the tissue to allow compressive global strain to occur, but the tension in the axons, dendrites and glial processes helps contain and resists the motion of the ECF. Therefore in the dynamic loading process, the local hydrostatic pressure in the ECF increases with the compressive force, and the tension in the axons, dendrites and glial processes also increases in a response to the hydrostatic pressure to maintain the

structure. Because direct experimental measurement of the stress–strain response of an axon under tensile loading at various strain rates is, to our knowledge, not available in the literature, we estimated the rate dependence using the Dennerll et al. (1989) viscoelastic model (a stiff spring in series with a Voigt element) for an axon under tension. Solving the differential equation using Matlab, we found that axons are predicted to stiffen a thousand-fold as strain rates are increased from 0.001/s to 1/s. In these non-equilibrium states, the field of local strains in the bulk tissue is heterogeneous, allowing pressure differences in the ECF.

The interaction between ECF hydrostatic pressure under compression and the tension in the axons, dendrites and glial processes is the common mechanism that may account for the change in the bulk tissue stress–stretch response at the various rates. Under quasi-static deformation, the tension in the axons, dendrites and glial processes is small so that substructure slip is possible, perhaps between axonal tracts or at interfaces of the different brain regions, as exhibited by the rapid stress drops and recoveries on our quasi-static stress–stretch curve. But at faster strain rates the tension in the stiffened axons, dendrites and glial processes is large enough to prevent such substructure slip so that the curves are smooth. At some global strain at the higher rates, the hydrostatic pressure in the ECF overcomes the resistance of the axons, dendrites and glial processes in many regions, perhaps because adhesions fail, cell membranes rupture, or tracts are rearranged, and allows more rapid ECF distribution that reduces the local hydrostatic pressure and thus the stress carrying ability of the tissue so that the stress curves cease to increase. The increased ECF flow correlates with the increase of the permeability values for the bulk tissue as a function of strain rate that we computed at the peak stress on our higher strain rate curves. Further evidence that the ECF can be moved by pressure differences is provided by studies of brain edema that state that the collection of edema fluid is due to a pressure gradient rather than diffusion (e.g. Reulen et al., 1977) and that edema fluid passage requires enlargement of the extracellular space.

One suggested cause of brain cell dysfunction is a transient increase in the plasma membrane permeability of neurons as a function of axonal tensile strain rate and strain magnitude (Geddes et al., 2003). Compressive loading of a neuronal–astrocytic culture at various strain rates immediately affects the cell membrane permeability and can lead to loss of electrochemical potential, osmotic imbalance, or cell rupture and death. The surviving damaged cells may have impaired axonal conduction or synapse firing (Cullen et al., 2011). The behavior of the ECF that we propose could be one immediate cause of the increase in axonal tension and thus may be a link between an external insult to the brain and cell damage.

In addition, in vivo deformation may damage the tissue structure by mechanically disrupting the neuronal–astrocytic connections, essential to communication for brain function (Fields and Stevens-Graham, 2002) and mediation of the inflammatory response to trauma (Myer et al., 2006), as well as by the more commonly assumed biochemical events. Communication of astrocytes with each other and with neurons in vivo involves modulated calcium signal transduction (Fiacco et al., 2009; Parpura and Haydon, 2000) that may be derailed by pathological behavior of the ECF.

4.2. *Deformation–relaxation tests*

The deformation–relaxation tests, originally intended to yield data from which the strain dependence of the permeability may be determined using the biphasic theory, fail to produce an estimate of the strain dependence of the permeability because the stress relaxation does not approach the equilibrium stress corresponding to the strain at the end of the ramp deformation. If the brain tissue response were similar to cartilage, the relaxation stress on the first cycle would approximate the stress on the quasi-static curve (Fig. 2a) at 0.95 stretch (5% global strain), which is much greater than zero. Instead, the load-relaxation tests in which the stress relaxes to zero provide further evidence that the compression-induced pressure on the ECF opens up extracellular space in a confined compression test.

The possibility that systematic experimental error exists in our apparatus and procedure was assessed and determined insignificant by similar tests of 1% agarose gel specimens that did not relax to zero stress. No separation was observed in the brain tests between the plunger and specimen. The relaxation of the stress to zero observed in our confined compression tests has also been observed in unconfined compression tests of brain tissue (Cheng and Bilston, 2007), as well as in indenter tests of larger specimens (Shafieian et al., 2009).

Load bearing soft tissues, which do not suffer significant mechanical damage under increasing deformation, relax much slower than brain tissue. Articular cartilage relaxation times to equilibrium are on the order of 3500 s (Soltz and Ateshian, 1998), and the annulus fibrosus of the intervertebral disc relaxes to equilibrium in about 5000 s (Périé et al., 2005). However, the deformable cartilage is both porous and permeable so that load-induced turgor pressures, caused by the entanglement of the collagen fibers and proteoglycan macromolecules, are dissipated slowly over time as fluid redistributes within the tissue. Because brain tissue stress relaxes much faster than cartilage at a set level of strain, brain tissue permeability is expected to be larger than that of cartilage since stress relaxation involves internal fluid redistribution in soft tissue and since damage increases permeability.

4.2.1. *Proposed role of solid–fluid interactions in the load-relaxation cycles*

The fluid content and structure of brain tissue provide a possible explanation of how the deformed tissue could relax to zero stress, but still support load on a subsequent increasing strain cycle. Because the tissue is in a non-equilibrium state during both deformation and stress relaxation, the internal forces are not balanced as they would be in equilibrium and a pressure gradient may exist in the fluid. The relaxation to zero stress under the confined compression boundary conditions cannot be explained by assuming the solid phase is viscoelastic, say a Maxwell fluid which relaxes to zero, because an undamaged viscoelastic solid must relax to a non-zero equilibrium state defined by the quasi-static tests. Although, the solid phase may well be better represented as viscoelastic rather than elastic, a question that we do not address in this work. If the relaxation to zero stress were due only to ECF transport from the specimen

rather than redistribution within the specimen, then the tissue would be unlikely to support stress on subsequent deformations.

Again, the structure of the undeformed brain tissue is maintained primarily by a combination of tension in neurites and glial processes that is balanced by hydrostatic pressure in the ECF (Van Essen, 1997), rather than any extracellular framework. At the end of the ramp deformation during which dynamic loading the system is in non-equilibrium states, the local strains are not uniformly distributed so that ECF hydrostatic pressure gradients exist in the tissue. During in vitro relaxation of brain tissue, these pressure differences induce ECF redistribution leaving axons, dendrites, and glial processes slack so that if the specimen relaxes to zero stress, the ECF hydrostatic pressures are zero, which is an equilibrium state. This description is consistent with the explanation given for cartilage stress relaxation by Holmes (1986) that the local strains do not become uniform until fluid redistributes within the specimen.

On a subsequent ramp deformation, the load-bearing axons, dendrites, and glial processes recover tension as the tissue fluid hydrostatic pressure increases as a result of the applied plunger compressive displacement so that the tissue specimen can again support force. The decline in peak stress on each subsequent cycle is a consequence of the solid–fluid interactions described in Section 4.1.1 for the ramp deformation. This behavior is another indication that the brain tissue response is deformation-history dependent, as well as rate-dependent.

4.3. *Limitations*

The limitations of the experiments may include the problem of maintaining physiologic water content and the size and heterogeneity of the specimens. As the alternative closest to in vivo conditions, it was decided to store the specimens in PBS during the less than 4 h from harvest to testing; therefore the tissue may contain slightly more fluid than in vivo. Not putting the tissue in PBS prior to sample testing would have allowed evaporation of up to 20% by weight over 3 h by our measurements in the 21 °C, 30% relative humidity lab environment. Such evaporation in air would compromise the investigation of the role of fluid in the mechanical response.

As in any post-mortem testing, biological tissue may degrade before testing due to cell death and bacterial growth. We minimized this influence on the mechanical properties by testing as quickly as possible.

The heterogeneous specimens are chosen to investigate the interaction of both medium scale and small-scale tissue substructures rather than the response of purely white or grey matter. A full mathematical model of the rat brain would probably require constitutive information about purely white matter, purely grey matter, and other small scale substructures. But even when such mathematical relations are obtained, further studies would be required to assemble such mathematical models to account for the mechanical interactions of the different regions of the brain. In this study, we sought to begin our investigation of the role of extracellular fluid by characterizing the bulk response in the chosen regions.

Some research groups have used much larger specimens obtained from larger animal brains. For example, the Miller-Chinzei (1997) sample is a swine cortex cylinder 30 mm in diameter and 10 mm high, a volume 74.4 times larger than the rat brain cylindrical specimens of diameter 6.35 mm and length 3 mm used here. The higher volume of the tissue tends to average out inhomogeneities or voids in the specimen and so the test results would be more likely to be reproducible than those from our small-sized samples. No method is available to scale the specimen size and correlate the results other than the stress–strain relation.

Our large specimen size with respect to the size of the full rat brain guarantees heterogeneity because it includes the interfaces between various subregions and so allows the results to have a more general application to the full brain response. Some published evidence shows that confinement of the brain tissue within the skull does influence mechanical response compared to in vitro tests of excised specimens (Gefen and Margulies, 2004) so that the confined compression test restriction of the ECF flow to some extent mimics confinement in the skull.

5. Conclusion

The confined compression tests suggest that trauma-induced increases in ECF hydrostatic pressure, which may induce pathological ECF flow, are one possible immediate mechanical cause of brain tissue damage. Interaction between the local ECF hydrostatic pressure and strain rate-dependent axonal stiffening is suggested as a mechanism to transmit external brain insults to the cellular level. In a confined compression test, the morphology of the loading curve is indicative of the interaction of solid elements with the ECF in the extracellular space of the tissue itself, as opposed to the motion of cerebrospinal fluid in the ventricles. The morphology suggests damage that is reflected in increased permeability at higher strain rates due to internal structural rearrangement that opens extracellular space to ECF flow, but that maintains much of the large-scale structural integrity of the tissue.

The loss in stress-carrying ability may be a consequence of cell rupture, disassociation of axonal–glial interconnections, relative motion of substructures in the heterogeneous tissue, or relative motion at interfaces or larger regions, etc, each of which may be a consequence of excessive hydrostatic pressure in the ECF. Our MRI investigation provides independent evidence of the structural damage suggested by the stress–stretch curves.

While we do not present a mathematical model for brain tissue here, we believe that these results show that a successful mathematical model for brain tissue under compression from insults must account for damage, perhaps through a damage parameter such as permeability, in the range from small to larger strains. However, the permeability as a function of strain and strain rate cannot be obtained from the load-relaxation technique as has been traditionally performed for cartilage because the standard biphasic theory employed for cartilage does not appear to apply to damaged brain tissue. The biphasic model is a continuum theory that assumes no damage beyond compaction during the deformation of the soft tissue, but the compressive properties of brain tissue change during the loading and relaxation.

Acknowledgments

This work was supported in part by a University of Maryland SEED grant and by the Center for Energetics Concepts Development of the University of Maryland-College Park.

REFERENCES

Ateshian, G.A., Warden, H., Kim, J.J., Grelsamer, R.P., Mow, V.C., 1997. Finite deformation biphasic material properties of bovine articular cartilage from confined compression experiments. Journal of Biomechanics 30, 1157–1164.

Bain, A.C., Meaney, D.F., 2000. Tissue-level thresholds for axonal damage in an experimental model of central nervous system white matter injury. Journal of Biomechanical Engineering 122, 615–622.

Bonneh-Barkay, D., Wiley, C.A., 2009. Brain extracellular matrix in neurodegeneration. Brain Pathology 19, 573–585.

Burgin, L.V., Aspden, R.M., 2008. Impact testing to determine the mechanical properties of articular cartilage in isolation and on bone. Journal of Materials Science: Materials in Medicine 19 (2), 703–711.

Cheng, S., Bilston, L.E., 2007. Unconfined compression of white matter. Journal of Biomechanics 40, 117–124.

Cullen, D.K., Vernekar, V.N., LaPlaca, M.C., 2011. Trauma-induced plasmalemma disruptions in three-dimensional neural cultures are dependent on strain modality and rate. Journal of Neurotrauma 28, 2219–2233.

Dennerll, T.J., Lamoureux, P., Buxbaum, R.E., Heidemann, S.R., 1989. The Cytomechanics of axonal elongation and retraction. The Journal of Cell Biology 109, 3073–3083.

Fiacco, T.A., Agulhon, C., McCarthy, K.D., 2009. Sorting out astrocyte physiology from pharmacology. Annual Review of Pharmacology and Toxicology 49, 151–174, http://dx.doi.org/10.1146/annurev.pharmtox.011008.145602.

Fields, R.D., Stevens-Graham, B., 2002. New insights into Neuron–Glia communication. Science 298 (5593), 556–562, http://dx.doi.org/10.1126/science.298.5593.556.

Franceschini, G., Bigonia, D., Regitnig, P., Holzapfel, G.A., 2006. Brain tissue deforms similarly to filled elastomers and follows consolidation theory. Journal of the Mechanics and Physics of Solids 54, 2592–2620.

Geddes, D.M., Cargill II, R.S., LaPlaca, M.C., 2003. Mechanical stretch to neurons results in a strain rate and magnitude-dependent increase in plasma membrane permeability. Journal of Neurotrauma 20, 1039–1049.

Gefen, A., Margulies, S.S., 2004. Are in vivo and situ brain tissues mechanically similar?. Journal of Biomechanics 37, 1339–1352.

Hilgetag, C.C., Barbas, H., 2006. Role of mechanical factors in the morphology of the primate cerebral cortex. PLoS Computational Biology 2 (3), e22 146–159.

Holmes, M.H., 1986. Finite deformation of soft tissue: analysis of a mixture model in uni-axial compression. Journal of Biomechanical Engineering 108, 372–381.

Kaczmarek, M., Subramaniam, R.P., Neff, S.R., 1997. The hydromechanics of hydrocephalus: steady-state solutions for cylindrical geometry. Bulletin of Mathematical Biology 59 (2), 295–323.

Liu, Q., Subhash, G., Moore, D.F., 2011. Loading velocity dependent permeability in agarose gel under compression. Journal of the Mechanical Behavior of Biomedical Materials 4, 974–982.

Miller, K., Chinzei, K., 1997. Constitutive modelling of brain tissue: experiment and theory. Journal of Biomechanics 30, 1115–1121.

Miller, K., Chinzei, K., 2002. Mechanical properties of brain tissue in tension. Journal of Biomechanics 35, 483–490.

Mow, V.C., Kuei, S.C., Lai, W.M., Armstrong, C.G., 1980. Biphasic creep and stress relaxation of articular cartilage in compression: theory and experiments. Journal of Biomechanical Engineering 102, 73–84.

Myer, D.J., Gurkoff, G.G., Lee, S.M., Hovda, D.A., Sofroniew, M.V., 2006. Essential protective roles of reactive astrocytes in traumatic brain injury. Brain 129, 2761–2772, http://dx.doi.org/10.1093/brain/awl165.

Noyes, F.R., Butler, D.L., Grood, E.S., Zernicke, R.F., Hefzy, M.S., 1984. Biomechanical analysis of human ligament grafts used in knee-ligament repairs and reconstructions. Journal of Bone and Joint Surgery, American 66 (3), 344–352.

Parpura, V., Haydon, P.G., 2000. Physiological astrocytic calcium levels stimulate glutamate release to modulate adjacent neurons. Proceedings of the National Academy of Sciences USA 97 (15), 8629–8634, http://dx.doi.org/10.1073/pnas.97.15.8629.

Périé, D., Korda, D., Iatridis, J.C., 2005. Confined compression experiments on bovine nucleus pulposus and annulus fibrosus: sensitivity of the experiment in the determination of compressive modulus and hydraulic permeability. Journal of Biomechanics 38, 2164–2171.

Prange, M.T., Margulies, S.S., 2002. Regional, directional, and age-dependent properties of the brain undergoing large deformation. Journal of Biomechanical Engineering 124, 244–252.

Prevost, T.P., Balakrishnan, A., Suresh, S., Socrate, S., 2011. Biomechanics of brain tissue. Acta Biomaterialia 7, 83–95.

Reulen, H.J., Graham, R., Spatz, M., Klatzo, I., 1977. Role of pressure gradients and bulk flow in dynamics of vasogenic brain edema. Journal of Neurosurgery 46, 24–35.

Shafieian, M., Darvish, K.K., Stone, J.R., 2009. Changes to the viscoelastic properties of brain tissue after traumatic axonal injury. Journal of Biomechanics 42, 2136–2142.

Shulyakov, A.V., Fernando, F., Cenkowski, S.S., Del Bigio, M.R., 2009. Simultaneous determination of mechanical properties and physiologic parameters in living rat brain. Biomechanics and Modeling in Mechanobiology 8, 415–425.

Simon, B.R., 1992. Multiphase poroelastic finite element models for soft tissue structures. Applied Mechanics Reviews 45, 191–218.

Simon, B.R., Kaufman, M.V., Liu, J., Baldwin, A.L., 1998. Porohyperelastic-transport-swelling theory, material properties and finite element models for large arteries. International Journal of Solids and Structures 35, 5021–5031.

Soltz, M.A., Ateshian, G.A., 1998. Experimental verification and theoretical prediction of cartilage interstitial fluid pressurization at an impermeable contact interface in confined compression. Journal of Biomechanics 31, 927–934 (2006) Corrigendum **39**, 594.

Strich, S., 1961. Shearing of nerve fibers as a cause of brain damage due to head injury. The Lancet 1961, 443–448.

Van Essen, D.C., 1997. A tension-based theory of morphogenesis and compact wiring in the central nervous system. Nature 385, 313–318.

Xu, G., Bayly, P.V., Taber, L.A., 2009. Residual stress in the adult mouse brain. Biomechanics and Modeling in Mechanobiology 8, 253–262.

Xu, G., Knutsen, A.K., Dikranian, K., Kroenke, C.D., Bayly, P.V., Taber, L.A., 2010. Axons pull on the brain, but tension does not drive cortical folding. Journal of Biomechanical Engineering 132 (7), 071013.